

RESEARCH PAPER

 OPEN ACCESS

## Metuzumab enhanced chemosensitivity and apoptosis in non-small cell lung carcinoma

Fei Feng<sup>a,\*</sup>, Bin Wang<sup>a,\*</sup>, Xiuxuan Sun<sup>a,\*</sup>, Yumeng Zhu<sup>a</sup>, Hao Tang<sup>b</sup>, Gang Nan<sup>a</sup>, Lijuan Wang<sup>a</sup>, Bo Wu<sup>a</sup>, Muren Huhe<sup>a</sup>, Shuangshuang Liu<sup>a</sup>, Tengyue Diao<sup>a</sup>, Rong Hou<sup>a</sup>, Yang Zhang<sup>a</sup>, and Zheng Zhang<sup>a</sup>

<sup>a</sup>National Translational Science Center for Molecular Medicine, Department of Cell Biology, Fourth Military Medical University, Xi'an, P.R. China; <sup>b</sup>Pacific Meinuoke Biopharmaceutical Company, Changzhou, P.R. China

### ABSTRACT

Targeted therapeutics is used as an alternative treatment of non-small cell lung cancer (NSCLC); however, treatment effect is far from being satisfactory, and therefore identification of new targets is needed. We have previously shown that metuzumab inhibit tumor growth *in vivo*. The present study was performed to investigate the anti-tumor efficacy of metuzumab combined with gemcitabine and cisplatin (GP), paclitaxel and cisplatin (TP) or navelbine and cisplatin (NP) regimens in multiple NSCLC cell lines. Our results demonstrate that, in comparison to single agent metuzumab or GP treated cells, metuzumab combined with GP display inhibitory effects on tumor growth. Furthermore, we found that metuzumab elevated the sensitivity of cell lines to gemcitabine, which was identified by MTT assay. Flow cytometric analysis showed that metuzumab combined with gemcitabine (GEM) treatment led to an obvious G1 arrest and an elevated apoptosis in A549, NCI-H460 and NCI-H520 cells. Western blot analysis also demonstrated a significantly reduced level of cyclin D1, Bcl-2, and an obviously increase level of Bax and full-length caspase-3 in A549, NCI-H460 and NCI-H520 cells treated with metuzumab/gemcitabine combination in comparison with single agent treated cells. In addition, metuzumab/gemcitabine treated A549, NCI-H460 and NCI-H520 cells also demonstrated a significantly increase in deoxycytidine kinase (dCK) protein level compared with single agent metuzumab or gemcitabine treated cells. Xenograft models also demonstrated that this metuzumab/gemcitabine combination led to upregulation of dCK. Taken together, the mechanisms of metuzumab combined with GP repress tumor growth were that the combined treatment significantly inhibited the tumor cell proliferation, apoptosis and cell cycle *in vitro* and *in vivo* and at least partially by induction of dCK expression. Our results suggested that metuzumab could significantly enhance chemosensitivity of human NSCLC cells to gemcitabine. Metuzumab/gemcitabine combination treatment may be a potentially useful therapeutic regimen for NSCLC patients.

**Abbreviations:** NSCLC, non-small cell lung cancer; GP, gemcitabine and cisplatin; TP, paclitaxel and cisplatin; NP, navelbine and cisplatin; MTT, 3-(4,5-Dimethylthiazol-2-yl)-2,5-diphenyltetrazolium bromide; GEM, gemcitabine; dCK, deoxycytidine kinase; MMPs, matrix metalloproteinases; ADCC, antibody-dependent cell-mediated cytotoxicity; CFDA, China Food and Drug Administration; dFdCTP, gemcitabine triphosphate; hlgG1, human IgG1; STR, short tandem repeat; TUNEL, Terminal deoxynucleotidyl transferase (TdT)-mediated dUTP nick end labeling; IOD, integrated optical density; dFdCDP, gemcitabine diphosphate; dCTP, deoxycytidine triphosphate; NOAEL, no observed adverse effect level

### ARTICLE HISTORY

Received 2 June 2016  
Revised 24 November 2016  
Accepted 18 December 2016

### KEYWORDS

CD147; chemosensitivity; gemcitabine; metuzumab; monoclonal antibody; non-small-cell lung cancer; targeted therapy

### Introduction


Lung cancer is one of the leading cause of cancer morbidity and mortality worldwide especially in China.<sup>1</sup> Approximately 80–85% of lung cancers are non-small cell lung cancers (NSCLCs) and the majority of patients with NSCLC have a poor prognosis.<sup>2</sup> The main treatments of lung cancer include surgical resection,<sup>3–5</sup> radiofrequency ablation,<sup>6</sup> radiotherapy,<sup>7</sup> platinum-based chemotherapies,<sup>8–11</sup> and targeted therapy.<sup>10,12–14</sup> Despite progress in the development for the treatment of NSCLC, only 15% of patients are expected to be alive at

5 years,<sup>7</sup> and has necessitated the development of targeted therapies.

CD147 is a highly glycosylated transmembrane protein that belongs to the immunoglobulin superfamily. Previously studies had shown that many malignant neoplasms highly express CD147,<sup>15</sup> especially in NSCLC.<sup>16</sup> Since aberrant expression of CD147 is associated with matrix metalloproteinases (MMPs) production,<sup>17</sup> tumorigenesis,<sup>18</sup> clinicopathological features,<sup>16,19</sup> invasion and metastasis,<sup>16</sup> poor prognosis<sup>19,20</sup> and chemoresistance,<sup>21</sup> it can be a potential candidate for target therapy.

**CONTACT** Yang Zhang  [zhengyangcerc@126.com](mailto:zhengyangcerc@126.com); Zheng Zhang  [zhangzy@aliyun.com](mailto:zhangzy@aliyun.com)  National Translational Science Center for Molecular Medicine, Department of Cell Biology, Fourth Military Medical University, Xi'an, 710032, P.R. China.

\*These authors contributed equally to this study.

 Supplemental data for this article can be accessed on the [publisher's website](#).

Published with license by Taylor & Francis Group, LLC © Fei Feng, Bin Wang, Xiuxuan Sun, Yumeng Zhu, Hao Tang, Gang Nan, Lijuan Wang, Bo Wu, Muren Huhe, Shuangshuang Liu, Tengyue Diao, Rong Hou, Yang Zhang, and Zheng Zhang

This is an Open Access article distributed under the terms of the Creative Commons Attribution-Non-Commercial License (<http://creativecommons.org/licenses/by-nc/3.0/>), which permits unrestricted non-commercial use, distribution, and reproduction in any medium, provided the original work is properly cited. The moral rights of the named author(s) have been asserted.

Metuzumab is an affinity-optimized and nonfucosylated anti-CD147 human-mouse chimeric IgG1 monoclonal antibody designed to reduce immunoreactivity and enhance antibody-dependent cell-mediated cytotoxicity (ADCC).<sup>22</sup> It has been approved to perform phase I clinical trial for NSCLC in China by China Food and Drug Administration (CFDA). Earlier pre-clinical studies of metuzumab combined with cisplatin and gemcitabine in xenograft mouse have demonstrated that this combination therapy was safe, tolerable and effectiveness. Additional studies evaluating the safety and efficacy of metuzumab in combination with various chemotherapeutic agents are ongoing.

In this study, we assess to the efficacy of metuzumab in combination with cisplatin dependent chemotherapy consisting of paclitaxel, navelbine and gemcitabine (GEM) as compared with chemotherapy alone in NSCLC xenograft mouse. Collectively, our results showed that metuzumab, in combination with cisplatin and gemcitabine, significantly enhanced the therapeutic efficacy in human NSCLC cells compared with single treatment, which may be associated with apoptosis induction and cell cycle arrest at G1 phase. Our results also indicated that metuzumab binding to CD147 promote the deoxycytidine kinase (dCK) expression level and may contribute to the gemcitabine metabolism to gemcitabine triphosphate (dFdCTP). Our results may support further evaluation of metuzumab in NSCLC patients, especially if subsets of patients more likely to benefit can be identified based on tumor molecule phenotype. However, the mechanism of metuzumab enhanced chemosensitivity of gemcitabine should be further studied.

## Results

### **Anti-proliferation activity of metuzumab combined with chemotherapy drugs in human NSCLC xenograft mice NSCLC cells**

To test efficacy of metuzumab combined with gemcitabine and cisplatin (GP), navelbine and cisplatin (NP) or paclitaxel and cisplatin (TP) in human NSCLC cell lines A549, NCI-H460 and NCI-H520 tumor xenograft model in nude mice, respectively. We treated the mice with saline, metuzumab, GP/TP/NP, or metuzumab combined with GP/TP/NP, and observed the development of tumors over a defined period. The tumor progression curves were shown in Fig. 1A. At the end of treatment, the average tumor volume of mice treated with the vehicle control increased by about 11.9-fold. The mean volume of tumors of the NSCLC cell xenografts treated with metuzumab or chemical drug alone were significantly smaller than those in the control groups (Table 1). We also found that metuzumab combined with NP did not significantly enhanced tumor toxicity compared with NP in A549 (54.40% vs. 53.01%,  $p = 0.8990$ ) and NCI-H460 (57.22% vs. 57.58%,  $p = 0.9154$ ) xenografts nude mice, metuzumab combined with TP neither enhanced tumor toxicity compared with TP in A549 (53.31% vs. 58.93%,  $p = 0.2353$ ) and NCI-H460 (58.80% vs. 57.28%,  $p = 0.3434$ ) xenografts nude mice, however, in NCI-H520 xenografts nude mice, a slight regression was found in

metuzumab combined with NP or TP group compared with NP or TP treatment alone (57.62% vs. 47.89%,  $p = 0.0056$  and 61.16% vs. 50.63%,  $p = 0.002$ ), respectively. Importantly, we noted that combination treatment with metuzumab and GP completely inhibited tumor growth in A549 xenograft model (91.89% vs. 71.01%,  $p < 0.001$  vs. GP), and a modest and statistically significant tumor growth inhibition compared with GP treated mice were found in NCI-H460 and NCI-H520 xenograft model (73.99% vs. 67.67%,  $p = 0.0001$  and 69.74% vs. 52.60%,  $p < 0.001$ , respectively), especially, in A549 xenografts nude mice, the mean tumor volume of metuzumab combined with GP even smaller than that of pre-treatment. Moreover, the level of metuzumab detected by immunohistochemistry staining represent the continued exposure of tumors to metuzumab at the end of experiments (Fig. 1C). All together, the antitumor activity of metuzumab combined with GP is better than those of metuzumab combined with TP or NP, and indicated that metuzumab could significantly improve the chemosensitivity of NSCLC cells to GP *in vivo*.

To determine the relationship between the level of CD147 and the anti-tumor efficacy, the CD147 expression level of the 3 NSCLC cell lines used in this work was determined by western blot (Fig. 2A), there were a greatest level of CD147 expression in NCI-H460 cells compared with A549 cells and NCI-H520 cells. The CD147 expression level was lowest in A549 cells among the 3 cell lines. The results was further confirmed by flow cytometry (Fig. 2B). However, these results showed the anti-tumor growth efficacy of metuzumab is independent of CD147 express level in these cell lines.

### **Metuzumab promoted GP-induced apoptosis and restrained tumor proliferation *in vivo***

To elucidate the mechanism of metuzumab combined with GP repress tumor growth, the tissue sections from each were collected, and assayed proliferation and apoptosis. To analyze cell proliferation status in the tumors, we assayed for the proliferative marker Ki-67 by using immunohistochemistry. The IOD value of Ki-67 of the mice treated with metuzumab combined with GP was significantly decreased from  $4191.12 \pm 680.92$  to  $1281.69 \pm 417.99$  in A549 cells ( $p < 0.001$ , Fig. 2C), from  $22713.76 \pm 2217.17$  to  $11098.13 \pm 1973.96$  in NCI-460 cells ( $p < 0.001$ , Fig. S1A, B) and from  $12873.21 \pm 1978.95$  to  $6604.58 \pm 971.51$  in NCI-H520 cells ( $p < 0.001$ , Fig. S2A, B), comparing to the mice treated with GP alone, indicating metuzumab combined with GP could remarkable inhibit the tumor cell proliferation compared with those treated with GP alone. Apoptosis was analyzed by an immunohistochemistry-based TUNEL assay. The percentage of apoptotic cells were increased in the metuzumab combined with GP group from  $34.32 \pm 13.11\%$  to  $49.71 \pm 16.09\%$  in A549 cells (Fig. 2C), from  $23.65 \pm 9.45\%$  to  $36.28 \pm 7.59\%$  in NCI-H460 cells (Fig. S1A, C), and from  $23.05 \pm 5.06\%$  to  $34.52 \pm 6.26\%$  in NCI-H520 cells (Fig. S2A, C). Furthermore, the upregulation of the apoptotic marker, Bax and downregulation of the survival marker, Bcl-2 were founded in metuzumab combined with GP group in A549 (Fig. 2C), NCI-H460 (Fig. S1A, D and E) and NCI-H520 (Fig. S2A, D and E) cells compared with those in control, metuzumab and GP group.

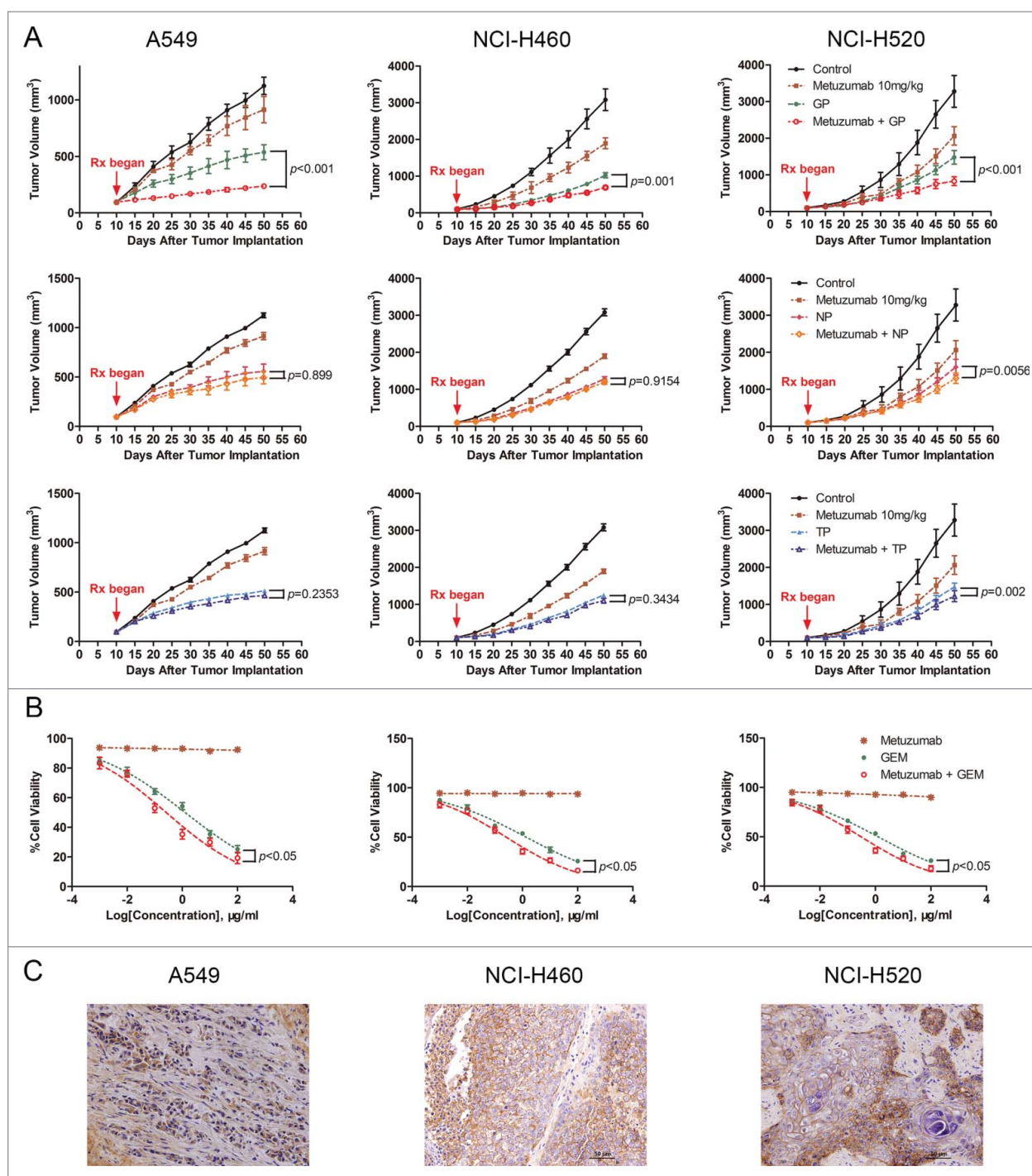


**Figure 1.** The antitumor efficacy of metuzumab combined with GP, TP or NP *in vitro* and *in vivo*. (A) Tumor growth inhibition with metuzumab alone or combined with GP, TP or NP in Balb/c nude mice bearing A549 (left), NCI-H460 (middle) and NCI-H520 (right) human lung cancer cell line xenografts. Data are presented as tumor volume (mm<sup>3</sup>) in the means  $\pm$  SD (n = 10). (B) Analysis of cell-growth rate by modified MTT assay. (C) Representative images of metuzumab distribution in nude mice bearing A549, NCI-H460 and NCI-H520 cell xenograft. Each experiment was repeated for at least 3 times.

### Metuzumab enhanced gemcitabine induced cell proliferation, apoptosis and cell cycle *in vitro*

Our previously study demonstrated that metuzumab is a non-fucosylate antibody, and promote antibody-dependent cellular cytotoxicity (ADCC) efficacy *in vivo*,<sup>22</sup> however, in this study, we found metuzumab apparently enhanced the antitumor efficacy of GP, but not satisfied to that of NP or TP. We speculated metuzumab enhanced chemosensitivity of NSCLC cells to GP is

not simply due to ADCC effect, nor cisplatin. To test this hypothesis, we evaluated the antitumor efficacy of metuzumab combined with gemcitabine *in vitro* without effect cells. MTT assay was performed and the results were analyzed to establish the dose-inhibition efficiency curves and calculate the IC<sub>50</sub> of metuzumab, GEM alone or combination to different NSCLC cells. As shown in Fig. 1B, metuzumab alone treatment cannot induce the cell death in NSCLC cell lines. The inhibition efficiencies of GEM, and metuzumab combined with GEM to

**Table 1.** The IR<sub>TV</sub> of metuzumab, GP, NP and TP alone or combination in xenografts nude mice.

	A549	NCI-H460	NCI-H520
metuzumab	39.34%	36.39%	35.18%
GP	71.01%	67.67%	52.60%
NP	53.01%	57.58%	47.89%
TP	58.93%	57.28%	50.63%
metuzumab combined with GP	91.89%	73.99%	69.74%
metuzumab combined with NP	54.40%	57.22%	57.62%
metuzumab combined with TP	53.31%	58.80%	61.16%

IR<sub>TV</sub>, inhibition ratio of tumor volume.

A549, NCI-H460, and NCI-H520 cells were significantly higher than those metuzumab treated cells ( $p < 0.05$ ), respectively. The IC<sub>50</sub> values were significantly decreased in the metuzumab

combined with GEM group, from 1.266  $\mu\text{M}$  to 0.262  $\mu\text{M}$  in A549 cells, from 1.371  $\mu\text{M}$  to 0.310  $\mu\text{M}$  in NCI-H460 cells, and from 1.251  $\mu\text{M}$  to 0.307  $\mu\text{M}$  in NCI-H520 cells, respectively, indicating that metuzumab could obviously enhance the chemosensitivity of NSCLC cells to gemcitabine. In addition, metuzumab alone did not inhibit PCNA expression, a cell proliferation marker, in A549, NCI-H460 and NCI-H520 cells, however, PCNA expression level significantly inhibited the cells treated with metuzumab combined with GEM, even compared with GEM treated cells (Fig. 3E).

To investigate the possible mechanisms of metuzumab in synergism of GEM, we treated A549, NCI-H460 and NCI-H520 cells with saline, human IgG1 (hIgG1), metuzumab, GEM or metuzumab combined with GEM and evaluated cell

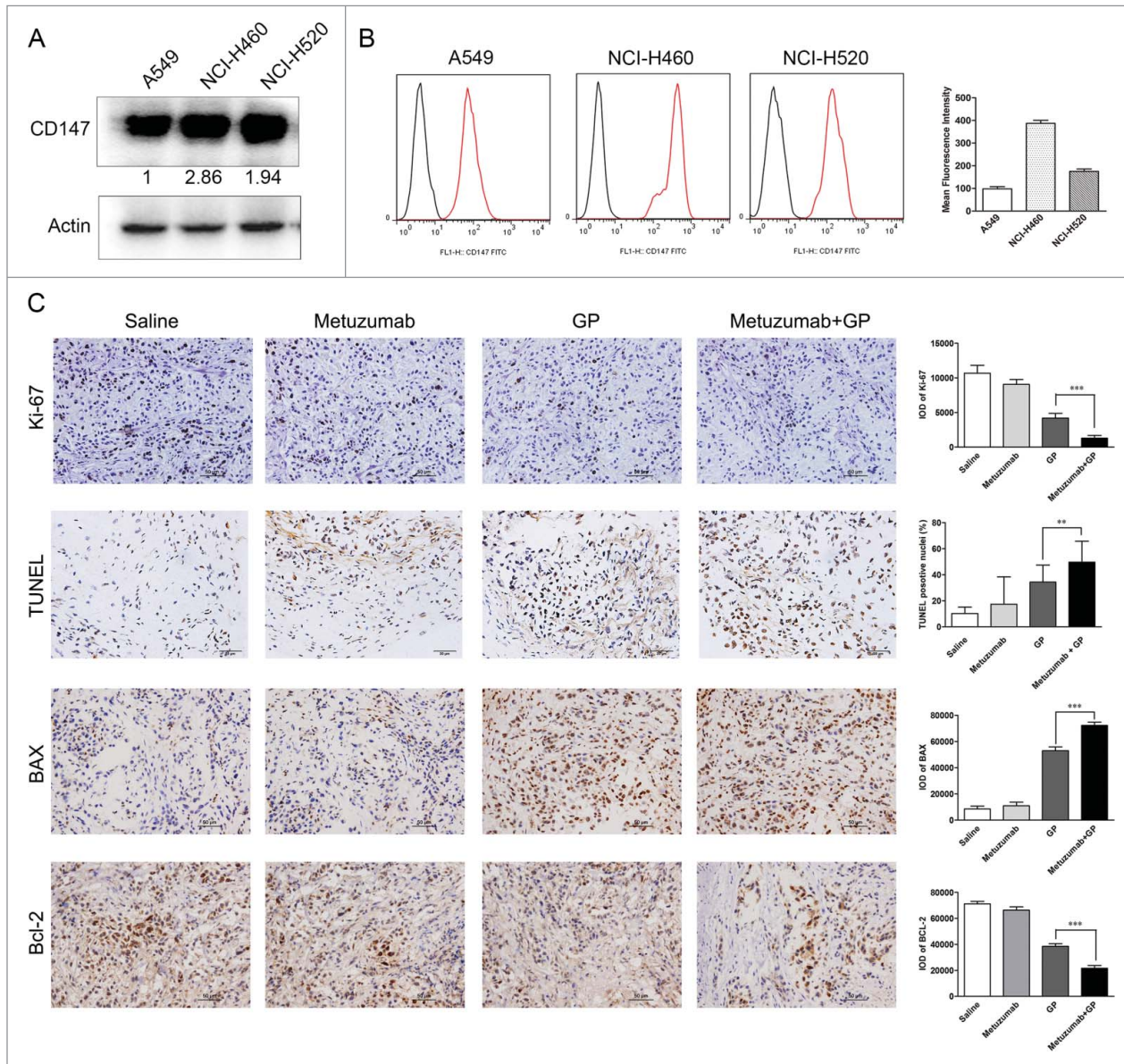


**Figure 2.** Metuzumab combined with GP represses cell proliferation and induces apoptosis *in vivo*. (A) Western blot analysis on the level of CD147 expression in A549, NCI-H460 or NCI-H520 cells.  $\beta$ -actin was used as the internal control. The experiments were performed triplicate. Gray-scale value was analyzed by Image J software for 3 times. The numbers indicate relative protein expression normalized to  $\beta$ -actin. (B) FACS analysis was used to examine the level of CD147 expression in A549, NCI-H460 or NCI-H520 cells. (C) Representative images of immunohistochemical staining for Ki-67, TUNEL, Bax and Bcl-2 in nude mice bearing A549 cell xenograft received metuzumab, GP or metuzumab combined with GP treatment. Scale bar in Ki-67, Bax and Bcl-2 represents 50  $\mu\text{m}$ , scale bar in TUNEL represents 20  $\mu\text{m}$ . Histogram represents the integrated optical density (IOD) of Ki-67, Bax and Bcl-2 expression and percentage of TUNEL positive nuclei from the studied group. The bars represent each sample performed in triplicate, and the error bars indicate mean  $\pm$  SD. \*\* $p < 0.01$ . \*\*\* $p < 0.001$ .

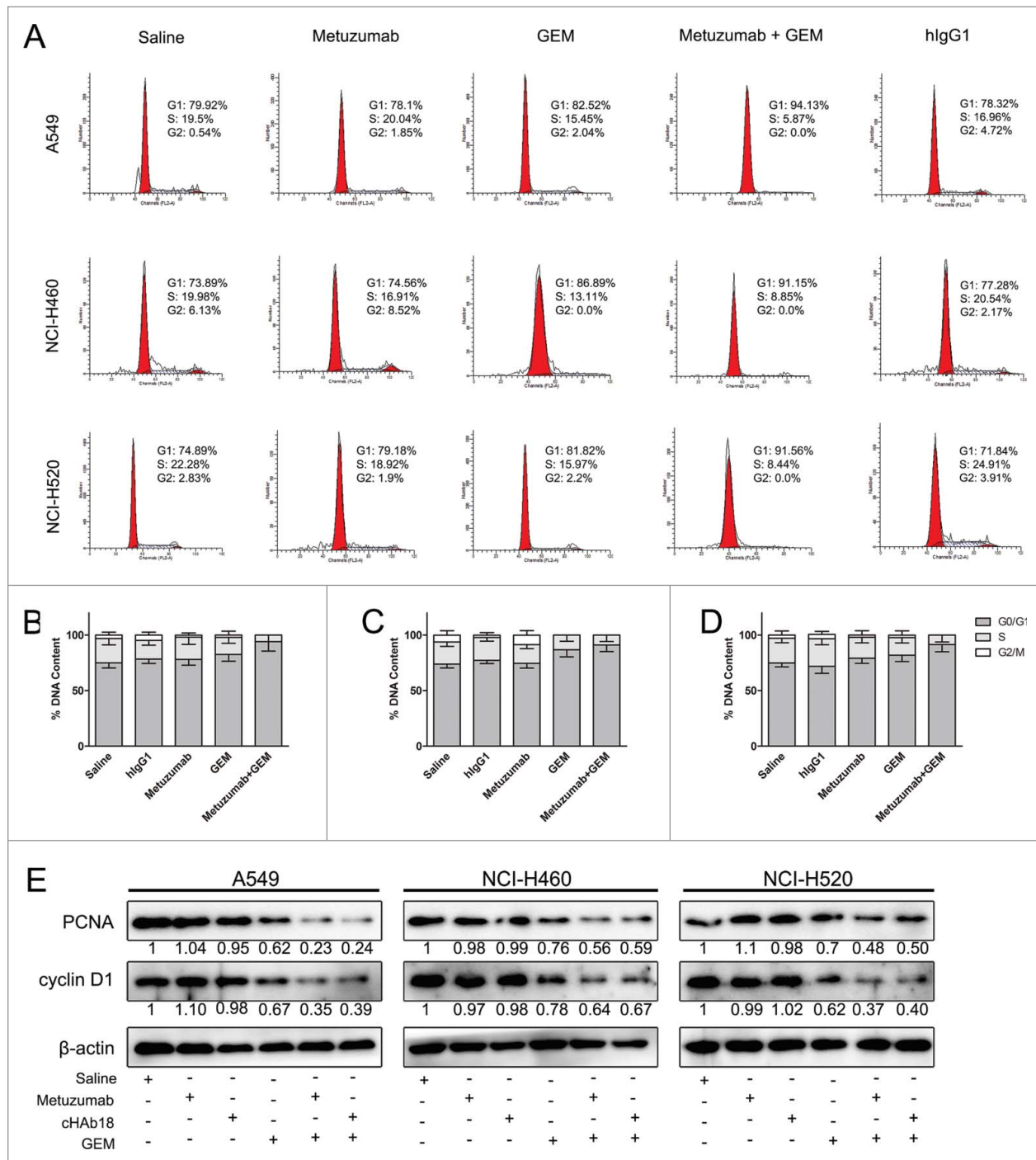


**Figure 3.** Combined effect of metuzumab and gemcitabine on cell cycle in A549, NCI-H460 and NCI-H520 cells. (A) Representative cell cycle profiles obtained by FACS analysis from propidium iodide stained A549, NCI-H460 or NCI-H520 cells treated with human IgG1, metuzumab, gemcitabine or metuzumab combined with gemcitabine. X-axis values correspond to DNA content; Y-axis values correspond to the number of events detected. Graph of the percentage of cells within each phase of the cell cycle in A549 (B), NCI-H460 (C) or NCI-H520 (D) cells obtained by FACS analysis. And data are presented as mean ± SD. (E) Western blot analysis on the expression levels of PCNA, cyclin D1 in A549, NCI-H460 or NCI-H520 cells treated with metuzumab or cHAb18, gemcitabine, and metuzumab or cHAb18 combined with gemcitabine for 24 hour. β-actin was used as the internal control. Gray-scale value was analyzed the same as above. The experiments were performed triplicate. The error bars indicate mean ± SD.

cycle using PI staining and flow cytometry. As shown in Fig. 3A-D, the percentages of A549, NCI-H460 and NCI-H520 cells treated with metuzumab and GEM at S phase were decreased moderately from 15.36% to 5.45% ( $p < 0.001$ ), 13.64% to 8.42% ( $p = 0.0002$ ) or 15.37% to 8.77% ( $p < 0.001$ ) comparing with the cells treated with GEM, and the percentages at G1 phase were increased significantly from 82.07% to 94.55% ( $p < 0.001$ ), 86.37% to 91.58% ( $p =$

0.005) or 82.11% to 91.23% ( $p < 0.001$ ), whereas, hIgG1 had no apparent effect on cell cycles. Furthermore, cyclin D1 (CCND1), a cell-cycle regulating gene and a G1/S transition checkpoint marker was found to be downregulated expression in metuzumab combined with GEM treatment groups than that in GEM treatment alone in 3 cell lines (Fig. 3E). All these results suggested that metuzumab combined with GEM lead to a moderate G1-phase arrest of NSCLC cells.

For metuzumab combined with GEM caused a significant arrest of G1 phase in NSCLC cells, we further examined the apoptosis rate of A549, NCI-H460 and NCI-H520 cells treated with saline, hIgG1, metuzumab, GEM and metuzumab combined with GEM for 24 hour by flow cytometry. As shown in Fig. 4A-D, the apoptosis rate of A549, NCI-H460 and NCI-H520 cells treated with metuzumab combined with GEM were significantly increased from 43.65% to 74.13%, from 41.09% to 69.24% and from 40.98% to 70.69%, respectively when comparing with A549, NCI-H460 and NCI-H520 cells treated with GEM alone, however, the hIgG1 had no inhibition of apoptosis to the 3 cell lines compare with the cells treated with saline. Furthermore, the western blot analysis showed a significant upregulation of Bax in NSCLC cells treated with metuzumab combined with GEM comparing with the cells treated with GEM alone (Fig. 4E). On the other hand, expression of Bcl-2 and full-length caspases-3 were downregulated in metuzumab combined with GEM treated cells in all the cell lines tested indicating apoptosis (Fig. 4E). All these results suggested metuzumab combined with GEM could significant improve the apoptosis rate of NSCLC cells. In additionally, although the apoptosis rate of A549, NCI-H460 and NCI-H520 cells treated with metuzumab were slightly increased from 2.35% to 11.12%, from 1.857% to 10.49%, and from 1.107% to 10.61% when comparing with the cells treated with saline (Fig. 4A-D), western blot analysis did not demonstrate metuzumab induces cell apoptosis (Fig. 4E). On the other hand, we assessed the effect of cHAb18 on cell cycle and apoptosis by western blot analysis. Consistent with metuzumab, cHAb18 combined with GEM regressed PCNA, cyclin D1 (Fig. 3E), Bcl-2 and full-length caspase-3 express level (Fig. 4E), and upregulation of Bax (Fig. 4E), comparing with the cells treated with GEM alone.

#### Augmentation of the cytotoxic effect of chemicals in NSCLC cells by metuzumab *in vitro* and *in vivo*

Deoxycytidine kinase (dCK) is a key rate-limiting enzyme response for conversion of GEM to active antimetabolite, the nucleotides gemcitabine diphosphate (dFdCDP) and triphosphate (dFdCTP). dFdCTP competes with endogenous deoxycytidine triphosphate (dCTP) for incorporation into newly synthesized DNA and inhibit DNA chain extends.<sup>23,24</sup> As metuzumab increased induction of apoptosis in response to GEM, we hypothesized that CD147 inhibition could promote conversion of gemcitabine to active metabolite by dCK. The A549, NCI-H460 and NCI-H520 cells were treated with 10  $\mu$ M hIgG1, cHAb18 or metuzumab. The expression level of dCK was determined by western blot analysis. An apparently increase in dCK was observed in metuzumab and cHAb18 treatment cells, the level of dCK increased about 3.15-fold in A549 cells, 2.11-fold in NCI-H460 cells and 2.96-fold in NCI-H520 cells treated with metuzumab, and increased about 3.11-fold, 2.09-fold and 2.88-fold in A549, NCI-H460 and NCI-H520 cells treated with cHAb18 antibody, respectively (Fig. 5A). In addition, the level of dCK in tumor obtained from metuzumab treated mice were determined by immunohistochemistry staining increased relative to the control group (Fig. 5B). Compared to the mouse in control group, the IOD of dCK value increased about 2.1-fold, 1.4-fold and 1.7-fold in

A549, NCI-H460 and NCI-H520 cells xenograft mouse treated with metuzumab, respectively. These results provided evidences that metuzumab promoted the expression of dCK might be partly responsible to the enhanced cytotoxicity of gemcitabine in CD147 overexpression NSCLC cells. However, the mechanism need to be further study on CD147 regulates dCK expression.

#### Discussion

Although non-small cell lung cancer (NSCLC) in humans remains incurable, available of alternative treatment regimens have contributed to inhibition of tumor growth and prolongation of survival of patients.<sup>25</sup> For example, gemcitabine combined with cisplatin (GP), paclitaxel combined with cisplatin (TP) and vinorelbine combined with cisplatin (NP) have been accept being first-line of treatment of NSCLC. However, the effect was not satisfactory, the further development for targeted drug therapy based on antibody is still needed.

Metuzumab is an afucosylated human/mouse chimeric IgG1 isotype monoclonal antibody that targets the CD147, which induced ADCC activation and enhanced anti-tumor effect. We have previously reported that metuzumab can inhibit NSCLC cells growth *in vitro* and *in vivo*.<sup>22</sup> Therapeutic mAbs are typically used in combination with one or more chemical drugs in the clinic.<sup>26</sup> To study the effectiveness of metuzumab combination chemotherapy in treating NSCLC and provide some evidences for clinical application, we evaluated the antitumor effect of metuzumab combination with common chemotherapeutic drugs including GP, TP or NP in human NSCLC A549, NCI-H460 and NCI-H520 cells xenograft mouse. Our results showed that metuzumab is effective in reducing the tumor growth in 3 NSCLC xenograft mouse. The tumor volumes were 39.4%, 36.39% and 35.18% in A549, NCI-H460 and NCI-H520 xenograft mouse administrated with metuzumab compared with the volumes of xenograft mouse treated with saline, respectively, which is accordance with our previously study.<sup>22</sup> Our results also indicated that metuzumab combined with GP could remarkable increase tumor inhibition rate in 3 NSCLC cells respectively, comparing with the cells treated with GP. However, metuzumab combined with NP or TP regimens did not enhanced tumor toxicity of NP or TP in A549 and NCI-H460 xenografts nude mice model, but a slight inhibit tumor growth of metuzumab combined with NP or TP were observed compared with that in NCI-H520 xenografts nude mice model treated with NP or TP (Fig. 1A). TUNEL results showed an elevated apoptosis rate of tumors generated from metuzumab combined with GP treated mice compared with that in metuzumab or GP group (Fig. 2C). These results suggestion metuzumab and GP interact synergistically to regress tumor growth *in vivo*.

To get a better understanding the mechanism by which metuzumab enhances the GP induced inhibition of tumor proliferation and apoptosis, we investigated the marker of key proteins known to regulate cell proliferation and apoptosis. We demonstrated that the level of Ki-67 and Bcl-2 protein were decreased and the level of Bax protein was increased in A549, NCI-H460 and NCI-H520 cells treated with either metuzumab or GP alone compared with control group. In addition, these

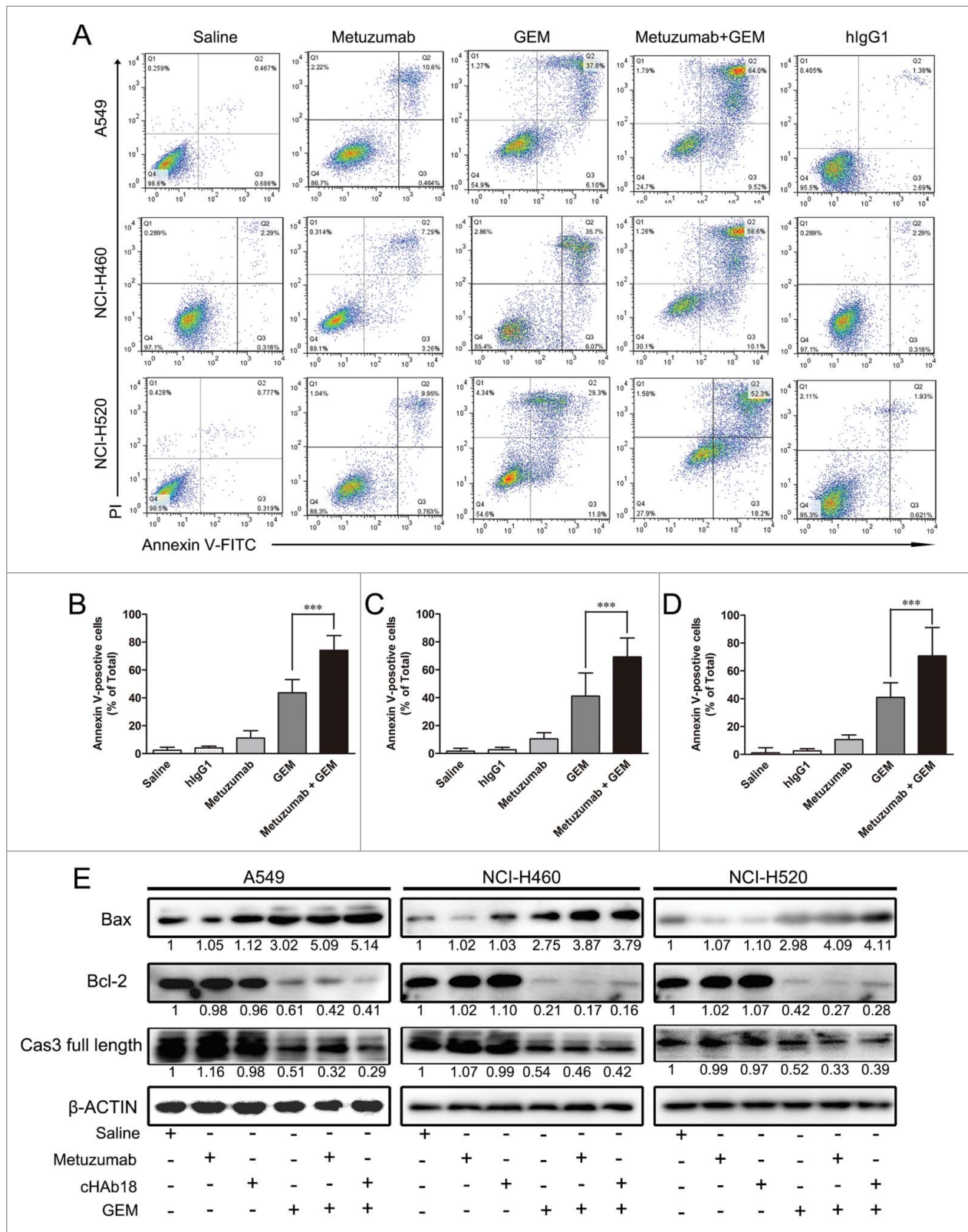


**Figure 4.** The effects of metuzumab combined with gemcitabine on apoptosis in A549, NCI-H460 and NCI-H520 cells. (A) Representative apoptosis profiles obtained by FACS analysis from Annexin V and propidium iodide stained in A549, NCI-H460 or NCI-H520 cells treated with human IgG1, metuzumab, gemcitabine or metuzumab combined with gemcitabine. Graphic presentation of data obtained from cell apoptosis analysis of A549 (B), NCI-H460 (C) or NCI-H520 (D) cells. Values are expressed as means (Q2+ Q3)  $\pm$  SD of at least 3 independent experiments. (E) Western blot analysis on the expression levels of Bax, Bcl-2 and full length caspase-3 in A549, NCI-H460 or NCI-H520 cells treated with metuzumab or cHAb18, gemcitabine and metuzumab or cHAb18 combined with gemcitabine for 24 hour.  $\beta$ -actin was used as the internal control. Gray-scale value was analyzed the same as above. The numbers indicate relative protein expression normalized to  $\beta$ -actin. The bars represent each sample performed in triplicate, and the error bars represent mean  $\pm$  SD. \*\*\* $p < 0.001$ .

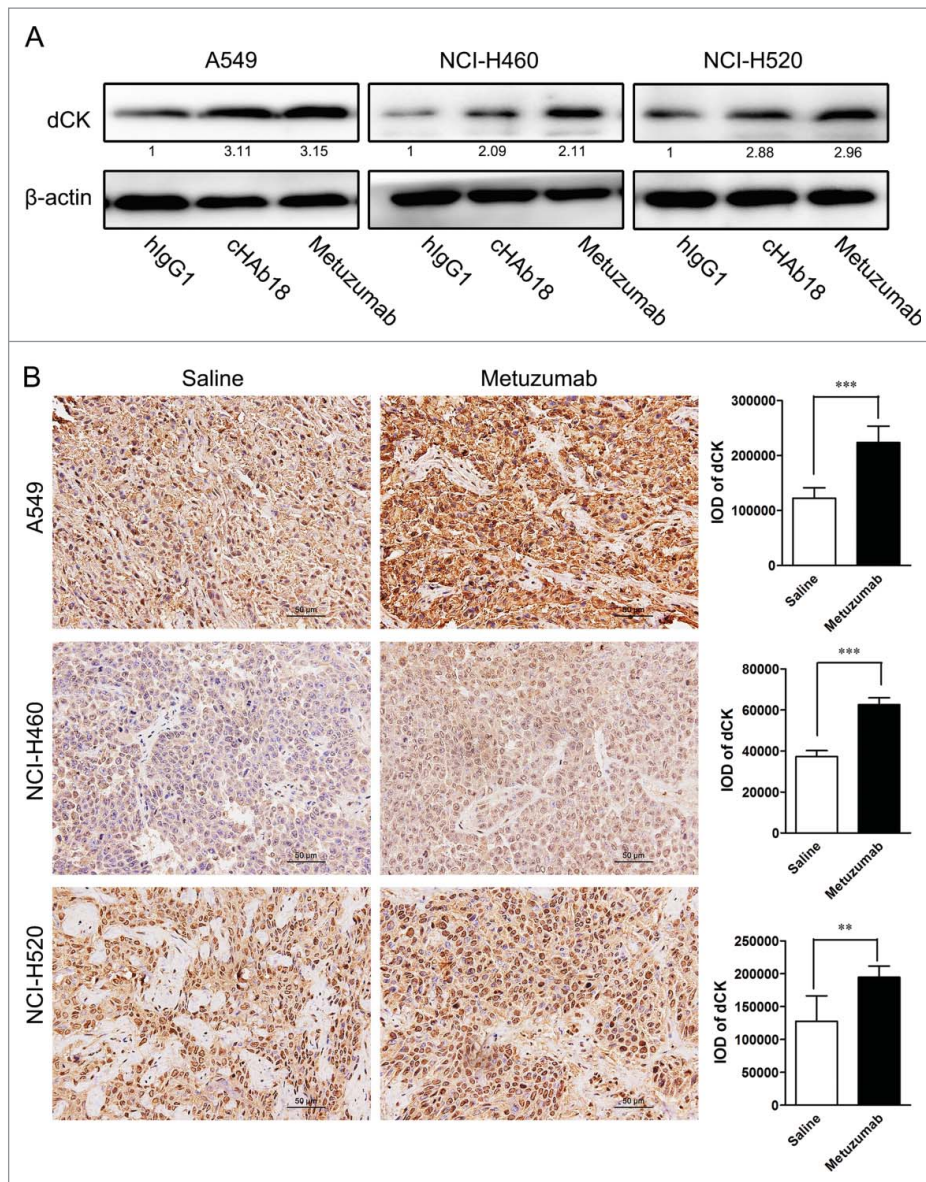


**Figure 5.** Metuzumab induces dCK expression *in vitro* and *in vivo*. (A) Western blot analysis on the level of dCK expression in A549, NCI-H460 or NCI-H520 cells treated with human IgG1, metuzumab or cHAb18 for 24 hour.  $\beta$ -actin was used as the internal control. Gray-scale value was analyzed the same as above. The numbers indicate relative protein expression normalized to  $\beta$ -actin. (B) Immunohistochemical staining for dCK expression in nude mice bearing A549 cell xenograft received saline or metuzumab treatment. Scale bar represents 50  $\mu$ m. Histogram represents the integrated optical density (IOD) of dCK expression. The bars represent each sample performed in triplicate, and the error bars indicate mean  $\pm$  SD. \*\* $p < 0.01$ . \*\*\* $p < 0.001$ .

changes in combination treatment group with metuzumab and GP were significantly greater than that in single treating group (Fig. 2C).

Furthermore, MTT analysis was performed when metuzumab or GEM was used individually and when those used in combination. Our results showed that compared with single agent GEM or metuzumab treatment, the cell death induced by metuzumab and GEM combination was significantly increased (Fig. 1B). This result indicated that the increase of anti-tumor effect of metuzumab combined with GP than that of GP possibly due to metuzumab promote GEM activity. Furthermore, cell cycle analysis and cell apoptosis detection were performed when metuzumab or GEM was used individually and when used in combination *in vitro*, but without effector cells, such as NK cell or peripheral blood mononuclear cell (PBMC). Our results showed that compared with single agent metuzumab or

GEM treatment, the G1/S phase accumulation and cell apoptosis induced by their combination was significantly increased, indicating that metuzumab enhances the GEM-induced cell cycle arrest and apoptosis on A549, NCI-460 and NCI-H520 cells (Fig. 3A-D and Fig. 4A-D).

Previous studies demonstrated that GEM inhibits the expression of cyclin D and Bcl-2, inducing G1 phase arrest in many types of human cancer cells including NSCLC.<sup>27-29</sup> Our results are consistent with these reports. The levels of cyclin D1 and Bcl-2 proteins were decreased in cells treated with GEM alone. In addition, these changes in combination treatment group with metuzumab and GEM were significantly greater than that in single treating group (Fig. 3E and Fig. 4E). On the other hand, it is known that Bax is an important protein that regulates the activation of caspase and leads cell to apoptosis.<sup>30</sup> Caspase-3 is regarded as one of the main executors of



apoptosis,<sup>31</sup> and reduction of full-length caspase-3 is correlated with apoptosis. We observed significant increase of Bax and inhibition of full length caspase-3 expression by metuzumab plus GEM treatment than that in single treating group (Fig. 4E). These *in vitro* and *in vivo* results can partly explain the enhanced effects of GEM-induced cell cycle arrest and apoptosis on cells by metuzumab.

Gemcitabine (or 2', 2'-difluorodeoxycytidine) is a pro-drug and a cytarabine analog that has been used widely as a chemotherapeutic agent for the treatment of multi-cancers.<sup>32</sup> It exerts cellular toxicity through the phosphorylated to its mononucleotide by dCK, and subsequently by nucleotide kinases to its active metabolites, such as dFdCDP and dFdCTP.<sup>33</sup> Accumulating evidences indicate that increase of dCK protein level<sup>34,35</sup> or activation of dCK<sup>36,37</sup> promote the antitumor effect of GEM. Our results showed for the first time that treatment of NSCLC cells with metuzumab can increase the expression of dCK *in vitro* and *in vivo*. As shown in Fig. 5, metuzumab treatment induced a 3.15-fold increase in A549 cells, 2.11-fold increase in NCI-H460 cells and 2.96-fold increase in NCI-H520 cells in dCK expression (Fig. 5A). And dCK level increased about 2.1-fold, 1.4-fold and 1.7-fold in A549, NCI-H460 and NCI-H520 cells xenograft mouse treated with metuzumab compared with that in control group (Fig. 5B), respectively. cHAb18 mAb, a fucosylated metuzumab, also enhanced dCK protein level (Fig. 5). These results suggested that binding to CD147 by metuzumab or cHAb18 is the main reason response of increase of dCK. However, the mechanism by which metuzumab induces expression of dCK remains elusive and needs to be further studied.

The potential off-target effect of mAb is attached to the red blood cells and cause hemolysis, and these effects exhibit species-specific properties.<sup>38</sup> In our preclinical study, metuzumab does not cause hemolysis in incubation with rabbit red blood cells (data not shown). No hemolysis and other several adverse reactions related to metuzumab were found in repeat-dose toxicity study in rats and cynomolgus monkeys, the no observed adverse effect level (NOAEL) were estimated to be 200 mg/kg in rats and in monkeys.<sup>22</sup> However, the safety studies and off-target effect of metuzumab should be considered carefully in clinical trial.

In summary, we had shown that metuzumab enhanced the efficacy of gemcitabine through upregulation of dCK protein level by binding to CD147, which lead to downregulated the expression of Bcl-2, cyclin D1 and full length caspase-3, and upregulated of Bax, thereby increasing cell apoptosis and G1 phase arrested. This investigation suggests a potential clinical application of the combination regimen for the treatment of NSCLC cancer patients.

## Materials and methods

### Cell culture

Human NSCLC cell lines A549, NCI-H520 and NCI-H460 were purchased from the American Type Culture Collection. Cells were cultured in RPMI-1640 medium (Sigma, St Louis, MO, USA) supplemented with 10% fetal bovine serum (Hyclone Laboratories, Logan, UT), 2 mmol/L L-glutamine, and 0.1mmol/L nonessential amino acids (Life Technologies),

and maintained at 37°C humidified atmosphere containing 5% CO<sub>2</sub>. Cell lines authentication were assessed using short tandem repeat (STR) DNA profiling method.

### Reagents

Metuzumab was generously provided by Pacific Meinuoke Biopharmaceutical Company (Changzhou, Jiangsu province, China) and diluted to certain concentration with sterile saline. Human IgG1 antibody was obtained from R&D Systems. Cisplatin was obtained from Qilu Pharmaceutical Co., Ltd. (China) and dissolved in sterile saline to a final concentration of 2 mg/mL. Gemcitabine was purchased from Eli Lilly and Company and dissolved in sterile saline to a final concentration of 200 mg/ml. Paclitaxel was obtained from Beijing SL Pharmaceutical Co., Ltd. (China) at a concentration of 6 mg/ml. Navelbine was provided from Pierre Fabre, Co., Ltd. (China) at a concentration of 10 mg/ml. All the chemicals were diluted in normal saline and dosed based on the weight of the mice receiving either treatment before each dosing regimen.

### Antitumor efficacy studies in Mice

Athymic nude mice (female, 5–6 weeks old) were purchased from Vital River Laboratories of China. Animals were housed (5 per cage) in specific pathogen-free (SPF) condition, supplied with food and water *ad libitum*, and kept on a 12 h light/dark cycle. All studies were conducted in accordance with the Institutional Animal Care and Use Committee approved protocols. Human NSCLC cancer cells ( $5 \times 10^6$ ) were suspended in Hank's balanced salt solution and implanted in the right dorsal flank of the mice. When tumors reached a mean volume of 100 mm<sup>3</sup>, mice were randomized into experimental groups (n = 10 or 6). Mice in different treatment received a single dose of metuzumab (10mg/kg), GP (100 mg/kg gemcitabine and 1 mg/kg cisplatin), TP (6.6 mg/kg paclitaxel and 1 mg/kg cisplatin), NP (4 mg/kg navelbine and cisplatin 1 mg/kg, NP), metuzumab combined GP (metuzumab 10 mg/kg, gemcitabine 100 mg/kg and cisplatin 1 mg/kg), metuzumab combined TP (metuzumab 10 mg/kg, paclitaxel 6.6 mg/kg and cisplatin 1 mg/kg), metuzumab combined NP (metuzumab 10 mg/kg, navelbine 4 mg/kg and cisplatin 1 mg/kg), and saline, respectively. Antibody injections were administered twice weekly and chemical drug injections one weekly. Mice treated with saline were represented as control group.

Tumors size were measured twice a week with a digital caliper using the following formula:  $(width^2 \times length)/2^{26}$ . Antitumor activity was assessed by calculating inhibition ratio of tumor volume (IR<sub>TV</sub>) based on medians by using following formula:  $[1 - \text{average RTV}_{\text{treatment}}(\text{day } x) / \text{average RTV}_{\text{control}}(\text{day } x)] \times 100\%$ .

### Methylthiazolyldiphenyl-tetrazolium bromide (MTT) assay

The effect of metuzumab, gemcitabine or the metuzumab/gemcitabine combination on cell viability were assessed by MTT assay as described previously.<sup>39,40</sup> Briefly,  $5 \times 10^3$  NSCLC cells (A549, NCI-H460 and NCI-H520) were seeded in 96-well plate and cultured in 24 h, metuzumab, gemcitabine, the

metuzumab/gemcitabine combination and saline were added to the cells. After additional 24h of respective treatments, 20  $\mu\text{L}$  of MTT (5 mg/ml) was added into the wells and cells were incubated for 4 hours. Media was removed and replaced with 100  $\mu\text{L}$  DMSO. Plate were read on a plate reader (BioRad Laboratories, Hercules, CA) at 490 nm, the reference wavelength was 690 nm. Inhibition of cell growth was measured as the percentage of viable cells relative to the control and calculated as follows: percent viable cells rate =  $100\% \times \text{OD}_T / \text{OD}_C$ , where  $\text{OD}_T$  is the average OD value of the treated samples, and  $\text{OD}_C$  is the average OD value of the control samples. The assay was repeated 3 times. The mean optical density ( $\text{OD} \pm \text{SD}$ ) was calculated for each group.

### Cell cycle and apoptosis analysis

Cell cycle and apoptosis were determined by flow cytometry. Cell cycle was determined using the Propidium Iodide (PtdIns) solution (Biolegend, San Diego, CA) according to the manufacturer's.  $4 \times 10^5$  cells were seeded in 6-well plates and treated with saline, hIgG1, metuzumab, gemcitabine and metuzumab plus gemcitabine, respectively. The cells were harvested at 24 hours after drug treatment and fixed with 70% ethanol. The cells were then resuspended with PBS containing 100  $\mu\text{g}/\text{mL}$  RNase and 50  $\mu\text{g}/\text{mL}$  propidium iodide (PtdIns). Cell cycle profiles of  $2 \times 10^5$  cells were analyzed using a FACScalibur flow cytometer (BD Biosciences).

Cell apoptosis was detected using the FITC-Annexin-V Apoptosis Detection Kit with PtdIns (Biolegend, San Diego, CA) according to manufacturer's. A total of  $4 \times 10^5$  cells were planted in 6-wells culture plates and treated with saline, hIgG1, metuzumab and GEM alone, or metuzumab combined with GEM, respectively, for 24 hours. Then the cells were collected, resuspended in 500  $\mu\text{l}$  binding buffer, and stained with 5  $\mu\text{l}$  Annexin V-FITC Conjugate and 10  $\mu\text{l}$  of PtdIns Solution. The stained cells ( $1 \times 10^5$ ) were then analyzed using a FACScalibur flow cytometer (BD Biosciences).

### Terminal deoxynucleotidyl transferase (TdT)-mediated dUTP nick end labeling (TUNEL) analysis

NSCLC tissues were fixed in 4% paraformaldehyde in PBS embedded in paraffin and cut into  $\sim 5\text{mm}$  sections through the center of the tissue. The sections were stained with terminal deoxynucleotidyl transferase (TdT)-mediated dUTP nick end labeling (TUNEL) analysis using the *in situ* cell-death detection kit (Keygen Bio-Technology Development Co., Ltd. Nanjing, China) following the manufacturer's protocol. The percentage of apoptotic cells were determined by counting at least 300 cells in 5 randomly selected fields<sup>41</sup> and calculated as the number of apoptotic cells per number of total cells  $\times 100\%$ .<sup>42</sup> The imaging of TUNEL staining were captured with an Olympus CX71 microscope (Olympus) and analysis using Image Pro Plus 6 software (Media Cybernetics, USA).

### Western Blotting

Cells were harvested and lysed with RIPA lysis buffer (Beyotime Biotechnology, China). The total proteins were quantified

by Bradford protein assay kit (PIERCE). The proteins were separated by SDS-PAGE and transferred into PVDF membrane. Membranes were blocked in blocking buffer (5% non-fat dry milk/0.1% Tween 20 in TBS) for 1h at room temperature, before being incubated at  $4^\circ\text{C}$  with the appropriate antibody in blocking buffer. The membranes were washed and incubated with the appropriated peroxidase conjugated secondary antibody. After washing, the proteins level was detected using ECL reagents (GE Healthcare). The following primary antibodies were used: anti-PCNA (Millipore, 1:250 dilution), anti-Bax (HangZhou HuaAn Biotechnology, China, 1:100 dilution), anti-Bcl-2 (Antibody Revolution, 1:250 dilution), anti-full length caspase-3 (Antibody Revolution, 1:100 dilution), and anti-dCK (Biorbyt, 1:500 dilution). Anti-rabbit (Pierce, 1:6000 dilution) or anti-mouse HRP-conjugated antibodies (Pierce, 1:3000 dilution) were used for secondary antibody reactions.

### Immunohistochemistry staining

Immunohistochemistry staining were performed using Biotin-Streptavidin HRP Detection kit (Zhongshan Bio, Beijing, China) according to the manufacturer's procedure.<sup>43</sup> in brief, tumor tissues obtained from A549, NCI-H460 and NCI-H520 nude mice xenografts were formalin-fixed, paraffin embedded, and then cut into 5- $\mu\text{m}$  sections. After antigen retrieval with autoclaving in citric acid, and inactivating endogenous peroxidase with 3%  $\text{H}_2\text{O}_2$ , the slides were incubated with the rabbit anti-mouse Ki67 monoclonal antibody (Abcam, 1:100 dilution), anti-Bax (HangZhou HuaAn Biotechnology, China, 1:100 dilution), anti-Bcl-2 (Antibody Revolution, 1:100 dilution) and anti-dCK (Biorbyt, 1:100 dilution) antibody overnight at  $4^\circ\text{C}$ . Second antibody conjugated with biotin was applied for 20 min at room temperature. To determine the distribution of metuzumab in tumor tissues, the slides were incubated with the biotin labeled goat anti-human antibody (ZSGB-BIO, China. 1: 150). The sections were developed in 3,3-diaminobenzidine(DAB) and counterstained with hematoxylin. The expression level was determined based on the integrated optical density (IOD) using Image Pro Plus 6 Software (Media Cybernetics, USA), according to the method described previously.<sup>44</sup>

### Flow cytometry assay

Levels of CD147 expression on the lung cancer cells (A549, NCI-H460 and NCI-H520) were determined by flow cytometry using a FITC mouse anti-CD147 antibody (BD Biosciences, 1:500 dilution) and a FITC mouse anti-human IgG1 antibody (abcam, 1:500 dilution) as an isotype control. Relative antigen expression is reported as median fluorescence intensity (MFI).<sup>22</sup>

### Statistical Analysis

For all cell line experiments, data were compiled from at least 3 independent experiments. All values are expressed as mean  $\pm$  SD., One-way ANOVA analysis followed by *t* test was used to evaluate differences between the individual groups. Graphpad

Prism 5 (San Diego, CA) was used for statistical analyses with  $p$  value < 0.05 were considered significant.

## Disclosure of potential conflicts of interest

No potential conflicts of interest were disclosed.

## Acknowledgments

The authors thanked Dr. Hao Tang and Dr. Qiang Feng (Pacific Meinoke Biopharmaceutical Company, Changzhou, Jiangsu province, China) for the provided of metuzumab. Ms. Xiying Yao and Ms. Liqing Xu assisted with cell culture.

## Funding

This work was supported in part by grants from National Basic Research Program (973 Program: 2015CB553701) and China National Science and Technology Major Project (2013ZX09301301).

## Author contributions

ZZ and YZ conceived and designed the study. FF, BW, XXS, YMZ and HT performed the in vitro experiments and analyzed the data. GN, LJW, BW, MRHH, SSL, TYD and RH performed animal studies. FF wrote the paper. ZZ and ZY revised the manuscript and accepted the final version. All authors read and approved the final manuscript.

## References

- Siegel R, Naishadham D, Jemal A. Cancer statistics, 2013. *CA: A Cancer J Clinicians* 2013; 63(1):11-30; PMID:23335087; <http://dx.doi.org/10.3322/caac.21166>
- Goldstraw P, Ball D, Jett JR, Le Chevalier T, Lim E, Nicholson AG, Shepherd FA. Non-small-cell lung cancer. *Lancet* 2011; 378(9804):1727-1740; [http://dx.doi.org/10.1016/s0140-6736\(10\)62101-0](http://dx.doi.org/10.1016/s0140-6736(10)62101-0)
- Spaks A, Svirina D, Spaka I, Jaunalksne I, Breiva D, Tracums I, Krievins D. CXCL4 chemokine ligand 4 (CXCL4) is predictor of tumour angiogenic activity and prognostic biomarker in non-small cell lung cancer (NSCLC) patients undergoing surgical treatment. *Biomarkers* 2016; 21(5):474-8:1-4; PMID:27098116; <http://dx.doi.org/10.3109/1354750X.2016.1172111>
- Stewart RL, Carpenter BL, West DS, Knifley T, Liu L, Wang C, Weiss HL, Gal TS, Durbin EB, Arnold SM, et al. S100A4 drives non-small cell lung cancer invasion, associates with poor prognosis, and is effectively targeted by the FDA-approved anti-helminthic agent niclosamide. *Oncotarget* 2016; 7(23):34630-42; PMID:27127879; <http://dx.doi.org/10.18632/oncotarget.8969>
- Xiao HQ, Tian RH, Zhang ZH, Du KQ, Ni YM. Efficacy of pemetrexed plus platinum doublet chemotherapy as first-line treatment for advanced nonsquamous non-small-cell-lung cancer: a systematic review and meta-analysis. *OncoTargets therapy* 2016; 9:1471-1476; PMID:27042115; <http://dx.doi.org/10.2147/OTT.S96160>
- Bhatia S, Pereira K, Mohan P, Narayanan G, Wangpaichitr M, Savaraj N. Radiofrequency ablation in primary non-small cell lung cancer: What a radiologist needs to know. *Indian J Radiol Imaging* 2016; 26(1):81-91; PMID:27081229; <http://dx.doi.org/10.4103/0971-3026.178347>
- Dinh TK, Fendler W, Chalubinska-Fendler J, Acharya SS, O'Leary C, Deraska PV, D'Andrea AD, Chowdhury D, Kozono D. Circulating miR-29a and miR-150 correlate with delivered dose during thoracic radiation therapy for non-small cell lung cancer. *Radiat Oncol* 2016; 11(1):61; PMID:27117590; <http://dx.doi.org/10.1186/s13014-016-0636-4>
- Sun XJ, Deng QH, Yu XM, Ji YL, Zheng YD, Jiang H, Xu YP, Ma SL. A phase II study of Endostatin in combination with paclitaxel, carboplatin, and radiotherapy in patients with unresectable locally advanced non-small cell lung cancer. *BMC Cancer* 2016; 16(1):266; PMID:27067521; <http://dx.doi.org/10.1186/s12885-016-2234-0>
- Kim HK, Cho JH, Choi YS, Zo JI, Shim YM, Park K, Ahn MJ, Ahn YC, Kim K, Kim J. Outcomes of neoadjuvant concurrent chemoradiotherapy followed by surgery for non-small-cell lung cancer with N2 disease. *Lung Cancer* 2016; 96:56-62; PMID:27133751; <http://dx.doi.org/10.1016/j.lungcan.2016.03.016>
- Berardi R, Rinaldi S, Santoni M, Newsom-Davis T, Tiberi M, Morgese F, Caramanti M, Savini A, Ferrini C, Torniai M, et al. Prognostic models to predict survival in patients with advanced non-small cell lung cancer treated with first-line chemo- or targeted therapy. *Oncotarget* 2016; 7(18):26916-24; PMID:27029035; <http://dx.doi.org/10.18632/oncotarget.8309>
- Franks SE, Jones RA, Briah R, Murray P, Moorehead RA. BMS-754807 is cytotoxic to non-small cell lung cancer cells and enhances the effects of platinum chemotherapeutics in the human lung cancer cell line A549. *BMC Res Notes* 2016; 9(1):134; PMID:26928578; <http://dx.doi.org/10.1186/s13104-016-1919-4>
- Feng L, Yao HP, Zhou YQ, Zhou J, Zhang R, Wang MH. Biological evaluation of antibody-maytansinoid conjugates as a strategy of RON targeted drug delivery for treatment of non-small cell lung cancer. *J Exp Clin Cancer Res* 2016; 35(1):70; PMID:27102688; <http://dx.doi.org/10.1186/s13046-016-0347-6>
- Zhou BO, Nie J, Yang W, Huang C, Huang YE, Zhao H. Effect of hydrothorax EGFR gene mutation and EGFR-TKI targeted therapy on advanced non-small cell lung cancer patients. *Oncology letters* 2016; 11(2):1413-1417; PMID:26893752; <http://dx.doi.org/10.3892/ol.2015.4066>
- Pallis AG, Serfass L, Dziadziusko R, van Meerbeek JP, Fennell D, Lacombe D, Welch J, Gridelli C. Targeted therapies in the treatment of advanced/metastatic NSCLC. *Eur J Cancer* 2009; 45(14):2473-2487; PMID:19596191; <http://dx.doi.org/10.1016/j.ejca.2009.06.005>
- Li Y, Xu J, Chen L, Zhong WD, Zhang Z, Mi L, Zhang Y, Liao CG, Bian HJ, Jiang JL, et al. HAb18G (CD147), a cancer-associated biomarker and its role in cancer detection. *Histopathology* 2009; 54(6):677-687; PMID:19438743; <http://dx.doi.org/10.1111/j.1365-2559.2009.03280.x>
- Xu X, Liu S, Lei B, Li W, Lin N, Sheng W, Huang A, Shen H. Expression of HAb18G in non-small lung cancer and characterization of activation, migration, proliferation, and apoptosis in A549 cells following siRNA-induced downregulation of HAb18G. *Mol Cell Biochem* 2013; 383(1-2):1-11; PMID:24013786; <http://dx.doi.org/10.1007/s11010-013-1722-7>
- Caudroy S, Polette M, Tournier JM, Bulet H, Toole B, Zucker S, Birembaut P. Expression of the extracellular matrix metalloproteinase inducer (EMMPRN) and the matrix metalloproteinase-2 in bronchopulmonary and breast lesions. *J Histochem Cytochem* 1999; 47(12):1575-1580; PMID:10567441
- Sidhu SS, Nawroth R, Retz M, Lemjabbar-Alaoui H, Dasari V, Basbaum C. EMMPRN regulates the canonical Wnt/beta-catenin signaling pathway, a potential role in accelerating lung tumorigenesis. *Oncogene* 2010; 29(29):4145-4156; PMID:20514014; <http://dx.doi.org/10.1038/onc.2010.166>
- Zhong X, Li M, Nie B, Wu F, Zhang L, Wang E, Han Y. Overexpressions of RACK1 and CD147 associated with poor prognosis in stage T1 pulmonary adenocarcinoma. *Annals Surg Oncol* 2013; 20(3):1044-1052; PMID:22592183; <http://dx.doi.org/10.1245/s10434-012-2377-4>
- Fei F, Li X, Xu L, Li D, Zhang Z, Guo X, Yang H, Chen Z, Xing J. CD147-CD98hc complex contributes to poor prognosis of non-small cell lung cancer patients through promoting cell proliferation via the PI3K/Akt signaling pathway. *Annals Surg Oncol* 2014; 21(13):4359-4368; PMID:25084765; <http://dx.doi.org/10.1245/s10434-014-3816-1>
- Zeng H, Qiu Y, Qu Y, Liang A, Deng A, Zhang W, Xiu B, Wang H, Wang H. Expression of CD147 in advanced non-small cell lung cancer correlated with cisplatin-based chemotherapy resistance. *Neoplasma* 2011; 58(5):449-454; PMID:21745000; [http://dx.doi.org/10.4149/neo\\_2011\\_05\\_449](http://dx.doi.org/10.4149/neo_2011_05_449)
- Zhang Z, Zhang Y, Sun Q, Feng F, Huhe M, Mi L, Chen Z. Preclinical pharmacokinetics, tolerability, and pharmacodynamics of metuzumab, a novel CD147 human-mouse chimeric and glycoengineered

- antibody. *Mol Cancer Therapeutics* 2015; 14(1):162-173; PMID:25376611; <http://dx.doi.org/10.1158/1535-7163.MCT-14-0104>
23. Mini E, Nobili S, Caciagli B, Landini I, Mazzei T. Cellular pharmacology of gemcitabine. *Annals Oncol* 2006; 17(Suppl 5):v7-12; PMID:16807468; <http://dx.doi.org/10.1093/annonc/mdj941>
  24. Huang P, Chubb S, Hertel LW, Grindey GB, Plunkett W. Action of 2',2'-difluorodeoxycytidine on DNA synthesis. *Cancer Res* 1991; 51(22):6110-6117; PMID:1718594
  25. de Carpeno JC, Baron MG, Aguiar J, Chacon JI, Feliu J, Garcia MJ, Madronal C, Colmenarejo A, Sanchez JJ, Ordonez A, et al. Biweekly regimen of cisplatin, gemcitabine and vinorelbine for advanced non-small-cell lung cancer. *Cancer Chemotherapy Pharmacol* 2006; 58(2):266-271; PMID:16308698; <http://dx.doi.org/10.1007/s00280-005-0143-z>
  26. He Q, Gao J, Ge S, Wang T, Li Y, Peng Z, Li Y, Shen L. Axitinib alone or in combination with chemotherapeutic drugs exerts potent antitumor activity against human gastric cancer cells *in vitro* and *in vivo*. *J Cancer Res Clin Oncol* 2014; 140(9):1575-1583; PMID:24804814; <http://dx.doi.org/10.1007/s00432-014-1693-4>
  27. Torres C, Linares A, Alejandro MJ, Palomino-Morales RJ, Delgado JR, Perales S. Interplay between gemcitabine and erlotinib over pancreatic adenocarcinoma cells. *Pancreas* 2016; 45(2):269-280; PMID:26495790; <http://dx.doi.org/10.1097/mpa.0000000000000452>
  28. Toyota Y, Iwama H, Kato K, Tani J, Katsura A, Miyata M, Fujiwara S, Fujita K, Sakamoto T, Fujimori T, et al. Mechanism of gemcitabine-induced suppression of human cholangiocellular carcinoma cell growth. *Int J Oncol* 2015; 47(4):1293-1302; PMID:26252371; <http://dx.doi.org/10.3892/ijo.2015.3118>
  29. Maseki S, Ijichi K, Nakanishi H, Hasegawa Y, Ogawa T, Murakami S. Efficacy of gemcitabine and cetuximab combination treatment in head and neck squamous cell carcinoma. *Mol Clin Oncol* 2013; 1(5):918-924; PMID:24649271; <http://dx.doi.org/10.3892/mco.2013.159>
  30. Pastorino JG, Chen ST, Tafani M, Snyder JW, Farber JL. The overexpression of Bax produces cell death upon induction of the mitochondrial permeability transition. *J Biol Chem* 1998; 273(13):7770-7775; PMID:9516487; <http://dx.doi.org/10.1074/jbc.273.13.7770>
  31. Persad R, Liu C, Wu TT, Houlihan PS, Hamilton SR, Diehl AM, Rashid A. Overexpression of caspase-3 in hepatocellular carcinomas. *Modern Pathol* 2004; 17(7):861-867; PMID:15098015; <http://dx.doi.org/10.1038/modpathol.3800146>
  32. Wong A, Soo RA, Yong WP, Innocenti F. Clinical pharmacology and pharmacogenetics of gemcitabine. *Drug Metab Rev* 2009; 41(2):77-88; PMID:19514966; <http://dx.doi.org/10.1080/03602530902741828>
  33. Plunkett W, Huang P, Gandhi V. Preclinical characteristics of gemcitabine. *Anti-Cancer Drugs* 1995; 6(Suppl 6):7-13; PMID:8718419
  34. Kerr M, Scott HE, Groselj B, Stratford MR, Karaszi K, Sharma NL, Kiltie AE. Deoxycytidine kinase expression underpins response to gemcitabine in bladder cancer. *Clin Cancer Res* 2014; 20(21):5435-5445; PMID:25224279; <http://dx.doi.org/10.1158/1078-0432.CCR-14-0542>
  35. Galmarini CM, Clarke ML, Jordheim L, Santos CL, Cros E, Mackey JR, Dumontet C. Resistance to gemcitabine in a human follicular lymphoma cell line is due to partial deletion of the deoxycytidine kinase gene. *BMC PHARMACOL* 2004; 4:8; PMID:15157282; <http://dx.doi.org/10.1186/1471-2210-4-8>
  36. Gregoire V, Rosier JF, De Bast M, Bruniaux M, De Coster B, Octave-Prignot M, Scalliet P. Role of deoxycytidine kinase (dCK) activity in gemcitabine's radioenhancement in mice and human cell lines *in vitro*. *Radiotherapy Oncol* 2002; 63(3):329-338; PMID:12142097; [http://dx.doi.org/10.1016/S0167-8140\(02\)00106-8](http://dx.doi.org/10.1016/S0167-8140(02)00106-8)
  37. Al-Katib AM, Aboukameel A, Ebrahim A, Beck FW, Tekyi-Mensah SE, Raufi A, Ahmed Y, Mandziara M, Kafri Z. Modulation of deoxycytidine kinase (dCK) and glycogen synthase kinase (GSK-3beta) by anti-CD20 (rituximab) and 2-chlorodeoxyadenosine (2-CdA) in human lymphoid malignancies. *Exp Hematol Oncol* 2014; 3:31; PMID:25937997; <http://dx.doi.org/10.1186/2162-3619-3-31>
  38. Nancy E, Nianyu L, Bailey K, Fort M, Stevenson R, Jawando R, Salyers K, Jawa V, Narayanan P, Stevens E, et al. Unexpected thrombocytopenia and anemia in cynomolgus monkeys induced by a therapeutic human monoclonal antibody. *Toxicol Pathol* 2013; 41(7):951-969; PMID:23475561; <http://dx.doi.org/10.1177/0192623312474727>
  39. Aras B, Yerlikaya A. Bortezomib and etoposide combinations exert synergistic effects on the human prostate cancer cell line PC-3. *Oncol Letters* 2016; 11(5):3179-3184; PMID:27123085; <http://dx.doi.org/10.3892/ol.2016.4340>
  40. Mohseni M, Samadi N, Ghanbari P, Yousefi B, Tabasinezhad M, Sharifi S, Nazemiyeh H. Co-treatment by docetaxel and vinblastine breaks down P-glycoprotein mediated chemo-resistance. *Iranian J Basic Medical Sci* 2016; 19(3):300-309; PMID:27114800
  41. Xiao TT, Wang YY, Zhang Y, Bai CH, Shen XC. Similar to spironolactone, oxymatrine is protective in aldosterone-induced cardiomyocyte injury via inhibition of calpain and apoptosis-inducing factor signaling. *PLoS One* 2014; 9(2):e88856; PMID:24551180; <http://dx.doi.org/10.1371/journal.pone.0088856>
  42. Bian HB, Pan X, Yang JS, Wang ZX, De W. Upregulation of microRNA-451 increases cisplatin sensitivity of non-small cell lung cancer cell line (A549). *J Exp Clin Cancer Res* 2011; 30:20; PMID:21329503; <http://dx.doi.org/10.1186/1756-9966-30-20>
  43. Hu Z, Lv G, Li Y, Li E, Li H, Zhou Q, Yang B, Cao W. Enhancement of anti-tumor effects of 5-fluorouracil on hepatocellular carcinoma by low-intensity ultrasound. *J Exp Clin Cancer Res* 2016; 35(1):71; PMID:27102814; <http://dx.doi.org/10.1186/s13046-016-0349-4>
  44. Elfayomy AK, Almasry SM, Attia GM, Habib FA. Enhanced expression of vascular endothelial growth factor and increased microvascular density in women with endometrial hyperplasia: a possible relationship with uterine natural killer cells. *Romanian J Morphol Embryol* 2015; 56(2 Suppl):725-734; PMID:26429165